

Antiscreening of the Ampère force in QED and QCD plasmas

Bastian Brandt

Institut für theoretische Physik, Universität Regensburg, D-93040 Regensburg

Anthony Francis, Harvey B. Meyer

*PRISMA Cluster of Excellence, Institut für Kernphysik and Helmholtz Institut Mainz,
Johannes Gutenberg-Universität Mainz, D-55099 Mainz, Germany*

(Dated: October 18, 2018)

The static forces between electric charges and currents are modified at the loop level by the presence of a plasma. While electric charges are screened, currents are not. The effective coupling constant at long distances is enhanced in both cases as compared to the vacuum, and by different amounts, a clear sign that Lorentz symmetry is broken. We investigate these effects quantitatively, first in a QED plasma and secondly using non-perturbative simulations of QCD with two light degenerate flavors of quarks.

PACS numbers: 12.38.Gc, 12.38.Mh, 52.27.Ep

I. INTRODUCTION

The properties of Abelian and non-Abelian plasmas are the subject of intensive experimental and theoretical investigation. See [1] for a recent overview of the status of research on the quark-gluon plasma, and [2] for a comparative discussion of Abelian and non-Abelian plasmas. Electromagnetic probes play an important role in heavy ion collision experiments, see for instance the recent [3, 4]. In particular, it is important to understand the way in which electromagnetic interactions are modified by the presence of a thermal medium. While calculating dynamical properties [5–8] is crucial to predicting experimental observables in heavy-ion collisions, here we will concentrate on static (time-independent) aspects of the electromagnetic force in a plasma.

It is well-known that the electric force is screened by the quasi-free charges of a plasma. This phenomenon of Debye screening occurs already in a plasma described by classical physics. The static force between currents however remains unscreened. The coupling constants of both forces are in fact enhanced at long distances as compared to the vacuum. In the vacuum, the intensity of the Coulomb force and the Ampère force are related, a consequence of Lorentz symmetry [9]. In a medium such as a plasma, they may have a different intensity. They receive a factor $(1 + e^2\kappa_\ell)$ and $(1 + e^2\kappa_t)$ respectively, where both κ_ℓ and κ_t are found to be positive and $\kappa_\ell > \kappa_t$. These coefficients are determined by the long-wavelength behavior of the static polarization tensor. An important point is that since the renormalized electromagnetic coupling is defined conventionally at long distances in the vacuum state (zero temperature), it is necessary to subtract the vacuum polarization tensor in order to obtain the medium-induced modification of the long-range force between renormalized charges and currents.

The enhancement of the effective coupling constant is perhaps physically more relevant in the case of currents, since the Ampère force remains unscreened. The enhancement of the latter can be understood intuitively, by noting that free charges that happen to be moving parallel to the external current line are attracted to it, thus reinforcing it, while free charges moving antiparallel are repelled. It is thus fair to speak of a medium-induced ‘antiscreening’ of the Ampère force. This picture is corroborated by the fact that the quantity κ_t , which quantifies the enhancement of the force, also enters the constitutive equation of the electric current at second order in a ‘hydrodynamic’ description, $\mathbf{j} = e\kappa_t\nabla \times \mathbf{B} + \text{other terms}$ [10].

As a potential QED application, consider the early universe in its first few minutes. There is a period where electrons and positrons, which are still relativistic, dominate the energy density along with photons, with comparatively few nucleons present. The protons can then be considered as slow-moving probes of the relativistic QED plasma. They interact at long distances via a Debye-screened potential. Its coefficient is modified by a factor $(1 + e^2\kappa_\ell)$. Note, however, that at the same order one also has to consider the two-photon exchange amplitude.

A coefficient analogous to κ_t has been introduced in the constitutive equation of shear stress [11], where it is denoted by κ . It multiplies a term that vanishes in flat space. It has been computed in the $SU(N)$ gauge theory at weak coupling in leading order [12] and has recently been addressed non-perturbatively using lattice Monte-Carlo simulations [13].

After deriving the physics interpretation of κ_ℓ and κ_t , we recall the known one-loop formulae for the polarization function in QED and extract the quantities κ_ℓ and κ_t (section II). The QCD case is simply obtained by multiplying the results by the number of colors carried by the quarks. In section III we then proceed to calculate for the first time the polarization function in the deconfined phase of QCD. We use Monte-Carlo simulations of lattice QCD with two

flavors of quarks (with the $O(a)$ improved Wilson action).

II. THEORY

In this section we define the correlation functions relevant to the calculation of the coefficients κ_ℓ and κ_t . We give their interpretation in subsection II B. In subsection II C, we review the role of κ_t as a second order coefficient in the constitutive equation of the electromagnetic current. Finally, we review the one-loop results for the polarization tensor and extract analytic representations for κ_ℓ and κ_t useful at small and at large fermion masses.

A. Definitions

We work in the Euclidean field theory. The vector current is defined as $j_\mu(x) = \bar{\psi}(x)\gamma_\mu\psi(x)$, where the Dirac matrices are all hermitian and satisfy $\{\gamma_\mu, \gamma_\nu\} = 2\delta_{\mu\nu}$. We define the polarization tensor as

$$\Pi_{\mu\nu}(q) \equiv \int d^4x e^{iq\cdot x} \langle j_\mu(x) j_\nu(0) \rangle. \quad (1)$$

In the vacuum, it is purely transverse,

$$\Pi_{\mu\nu}^{\text{vac}}(q) = P_{\mu\nu}(q)q^2\Pi^{\text{vac}}(q^2), \quad (2)$$

$$P_{\mu\nu}(q) = q_\mu q_\nu / q^2 - \delta_{\mu\nu}. \quad (3)$$

With these conventions, the spectral function

$$\rho^{\text{vac}}(s) \equiv -2 \text{Im} \Pi^{\text{vac}}(-s - i\epsilon) \quad (s \geq 0) \quad (4)$$

is non-negative for a flavor-diagonal correlator. For the electromagnetic current, it is related to the R ratio via

$$\rho^{\text{vac}}(s) = \frac{R(s)}{6\pi}, \quad R(s) \equiv \frac{\sigma(e^+e^- \rightarrow \text{hadrons})}{4\pi\alpha(s)^2/(3s)}. \quad (5)$$

The denominator is the treelevel cross-section $\sigma(e^+e^- \rightarrow \mu^+\mu^-)$ in the limit $s \gg m_\mu^2$, and we have neglected QED corrections.

At finite temperature $T \equiv 1/\beta$, the tensor decomposition reads

$$\Pi_{\mu\nu}(q) = P_{\mu\nu}^L(q) \Pi_L(q_0^2, \mathbf{q}^2) + P_{\mu\nu}^T(q) \Pi_T(q_0^2, \mathbf{q}^2), \quad (6)$$

where $P_{00}^T(q) = 0 = P_{0i}^T(q) = P_{i0}^T(q)$ and $P_{ij}^T(q) = q_i q_j / \mathbf{q}^2 - \delta_{ij}$, while $P_{\mu\nu}^L(q) = P_{\mu\nu}(q) - P_{\mu\nu}^T(q)$.

We define the ‘matter’ part of the polarization tensor via

$$\Pi_{\mu\nu}(q) \equiv \Pi_{\mu\nu}^{\text{vac}}(q) + \Pi_{\mu\nu}^{\text{mat}}(q), \quad (7)$$

$$\Pi_L^{\text{mat}}(q) \equiv \Pi_L(q) - q^2 \Pi^{\text{vac}}(q^2), \quad (8)$$

$$\Pi_T^{\text{mat}}(q) \equiv \Pi_T(q) - q^2 \Pi^{\text{vac}}(q^2). \quad (9)$$

With these conventions, following [10] we define

$$\kappa_t = - \left. \frac{\partial}{\partial(q_3^2)} \Pi_{11}^{\text{mat}}(q_3 \mathbf{e}_3) \right|_{q_3=0} = \left. \frac{\partial}{\partial(\mathbf{q}^2)} \Pi_T^{\text{mat}}(0, \mathbf{q}^2) \right|_{\mathbf{q}=0}, \quad (10)$$

$$\kappa_\ell = - \left. \frac{\partial}{\partial(q_3^2)} \Pi_{00}^{\text{mat}}(q_3 \mathbf{e}_3) \right|_{q_3=0} = \left. \frac{\partial}{\partial(\mathbf{q}^2)} \Pi_L^{\text{mat}}(0, \mathbf{q}^2) \right|_{\mathbf{q}=0}. \quad (11)$$

We now turn to the interpretation of these quantities.

B. Interpretation of κ_ℓ and κ_t

Consider an $SU(3) \times U(1)$ vector gauge theory with quarks as the only matter fields. Let S be the action of quarks (described by the field $\psi(x)$), gluons ($A_\mu(x)$) and photons ($B_\mu(x)$). The partition function of the system coupled to a classical electromagnetic source $J_\mu(x)$ (it satisfies $\partial_\mu J_\mu(x) = 0$) reads

$$Z[J] = \int D[\bar{\psi}]D[\psi] D[A] D[B] \exp\left(-S - ie_0 \int d^4x B_\mu(x)J_\mu(x)\right). \quad (12)$$

Expanding the free energy $F[J] = -\frac{1}{\beta} \log Z[J]$ in J , one obtains for the quadratic term

$$F^{(2)}[J] = \frac{e_0^2}{2\beta} \int d^4x \int d^4y \langle B_\mu(x)B_\nu(y) \rangle_{J=0} J_\mu(x)J_\nu(y). \quad (13)$$

1. Free energy of electromagnetic sources at zero-temperature

Consider first the situation at zero temperature. In one loop approximation in the electromagnetic coupling e , the photon propagator is such that

$$\int d^4x J_\mu(x) \langle B_\mu(x)B_\nu(y) \rangle_{J=0} = \int d^4x J_\mu(x) \int \frac{d^4q}{(2\pi)^4} \frac{\delta_{\mu\nu} e^{iq(x-y)}}{q^2(1 - e_0^2 \Pi^{\text{vac}}(q^2))}. \quad (14)$$

For a static source of the form

$$J_0(x) = Q_1 \delta^{(3)}(\mathbf{x}) + Q_2 \delta^{(3)}(\mathbf{x} - \mathbf{r}), \quad J_i(x) = 0, \quad (15)$$

$F^{(2)}[J]$ can be interpreted as the static potential between two static U(1) charges. As a check that one recovers the familiar expression, for the source (15) the quadratic contribution to the free energy becomes

$$F^{(2)}(r) = V(r) = Q_1 Q_2 \int \frac{d^3\mathbf{q}}{(2\pi)^3} \frac{e_0^2}{1 - e_0^2 \Pi^{\text{vac}}(q^2)} \frac{e^{i\mathbf{q}\cdot\mathbf{r}}}{q^2} + \dots \quad (16)$$

where the remaining terms are independent of \mathbf{r} . The renormalization of the electric charge leads to the substitution

$$\frac{e_0^2}{1 - e_0^2 \Pi^{\text{vac}}(q^2)} = \frac{e^2}{1 - e^2 [\Pi^{\text{vac}}(q^2) - \Pi^{\text{vac}}(0)]} \quad (17)$$

at one-loop accuracy. We have thus recovered the familiar expression of the Coulomb potential, modified by the vacuum polarization [14], the so-called Uehling potential.

2. Generalization to finite temperature

In momentum space, the (00) component of the static (i.e. $q_0 = 0$) photon propagator is given at one loop by

$$\int d^4x e^{-i\mathbf{q}\cdot(\mathbf{x}-\mathbf{y})} \langle B_0(x)B_0(y) \rangle_{J=0} = \frac{1}{q^2 - e_0^2 \Pi_L(0, q^2)}. \quad (18)$$

Since the electric charge is conventionally renormalized at zero temperature, the free energy added by the presence of the two static leptons is given by

$$F_l^{(2)}(r) = Q_1 Q_2 \int \frac{d^3\mathbf{q}}{(2\pi)^3} \frac{e_0^2}{q^2 - e_0^2 \Pi_L(0, q^2)} e^{i\mathbf{q}\cdot\mathbf{r}} \quad (19)$$

$$= Q_1 Q_2 \int \frac{d^3\mathbf{q}}{(2\pi)^3} \frac{e^2}{1 - e^2 [\Pi_L^{\text{mat}}(0, q^2)/q^2 + \Pi^{\text{vac}}(q^2) - \Pi^{\text{vac}}(0)]} \frac{e^{i\mathbf{q}\cdot\mathbf{r}}}{q^2}. \quad (20)$$

Given the expansion at small momenta

$$\Pi_L^{\text{mat}}(0, q^2) = -\chi_s + \kappa_l q^2 + \dots, \quad (21)$$

and $\Pi^{\text{vac}}(\mathbf{q}^2) - \Pi^{\text{vac}}(0) = \mathcal{O}(\mathbf{q}^2)$, the Coulomb potential is screened at long distances, with a screening mass given by

$$m_{\text{el}}^2 = e^2 \chi_s. \quad (22)$$

Explicitly, the interaction free energy is given at long distances by

$$F_l^{(2)}(r) = \frac{e^2}{1 - e^2 \kappa_l} \frac{Q_1 Q_2 e^{-m_{\text{el}} r}}{4\pi r}. \quad (23)$$

Consider now the stationary source

$$iJ_3(x) = I_1 \delta^{(2)}(\mathbf{x}_\perp) + I_2 \delta^{(2)}(\mathbf{x}_\perp + \mathbf{R}_\perp), \quad \mathbf{x}_\perp \equiv (x_1, x_2), \quad (24)$$

where the other components of J_μ vanish. It describes two long wires along the \mathbf{e}_3 direction (which we take to be length L_3), separated by a distance $|\mathbf{R}_\perp|$. The currents I_1 and I_2 correspond to the charge, measured in units of e , that flows per unit time along the \mathbf{e}_3 direction. Then, up to $|\mathbf{R}_\perp|$ -independent terms,

$$F_t^{(2)}(R_\perp) = -I_1 I_2 L_3 \int \frac{d^2 \mathbf{q}_\perp}{(2\pi)^2} \frac{e_0^2}{\mathbf{q}_\perp^2 - e_0^2 \Pi_T(\mathbf{q}_\perp^2)} e^{i\mathbf{q}_\perp \cdot \mathbf{R}_\perp} \quad (25)$$

$$= -I_1 I_2 L_3 \int \frac{d^2 \mathbf{q}_\perp}{(2\pi)^2} \frac{e^2}{1 - e^2 [\Pi_T^{\text{mat}}(\mathbf{q}_\perp^2)/\mathbf{q}_\perp^2 + \Pi^{\text{vac}}(\mathbf{q}_\perp^2) - \Pi^{\text{vac}}(0)]} \frac{e^{i\mathbf{q}_\perp \cdot \mathbf{R}_\perp}}{\mathbf{q}_\perp^2} \quad (26)$$

Thus we see that the transverse channel Π_T modifies Ampère's $1/R_\perp$ force law. At long distances, the modification is given by

$$-\frac{1}{L_3} \frac{\partial F_t^{(2)}}{\partial R_\perp} = -\frac{e^2}{1 - e^2 \kappa_t} \cdot \frac{I_1 I_2}{2\pi R_\perp}. \quad (27)$$

Thus a positive value of κ_t corresponds to an enhancement of the strength of the $1/R_\perp$ force law, as compared to the Ampère force in the vacuum.

C. Constitutive equation of the electromagnetic current

The equation of continuity for the electric charge, $\dot{\rho} + \nabla \cdot \mathbf{j} = 0$, can be used to describe the time evolution of a non-equilibrium initial charge distribution. This ‘hydrodynamic’ description applies on long distance and time scales. It needs to be supplemented by a constitutive equation in order to be predictive. At lowest order in a derivative expansion, $e\mathbf{j} = \sigma \mathbf{E} - eD\nabla\rho$, with the conductivity σ and the diffusion coefficient related by $\sigma = \chi_s D$. At the next order, the most general allowed terms are of the form [10]

$$(1 + \tau_J \partial_t) e\mathbf{j} = -eD\nabla\rho + \sigma \mathbf{E} + \kappa_B \nabla \times \mathbf{B}. \quad (28)$$

Note that in our conventions, for the QCD plasma σ and κ_B are both of order e^2 in the electromagnetic coupling. Through the linear response formalism, one shows [10] that the coefficient multiplying the the curl of \mathbf{B} is directly related to the quantity $\kappa_t = \kappa_B/e^2$ introduced above from the medium-induced part of the polarization function Π_T^{mat} .

Equation (28) confirms the interpretation that the coefficient $\kappa_t > 0$ corresponds to an antiscreening of electric currents in the medium. Indeed, suppose an external current $I_0 = I_{\text{ext}}$ flowing along a straight line is applied to the system, creating circular magnetic field lines around it. If we choose a transverse disc S (with an edge ∂S) centered on it, the response electric current $e \int_S d\sigma \cdot \mathbf{j}$ flowing through S is given by $I_1 = \kappa_B \int_{\partial S} d\ell \cdot \mathbf{B}$. This current enhances the circulation of the magnetic field along ∂S by an amount equal to I_1 , which in turn induces a current I_2 . This amounts to a geometric series $\sum_{k=0}^{\infty} I_k$, so that the net effect is to enhance I_0 by a factor $1/(1 - \kappa_B)$.

D. Leading-order perturbative results

We now give one-loop results for the polarization tensor and its small \mathbf{q}^2 expansion in a pure QED plasma with one Dirac fermion of mass m carrying a charge e . The expressions for QCD are obtained by summing the contribution of each quark flavor and multiplying the result by the number of colors N_c .

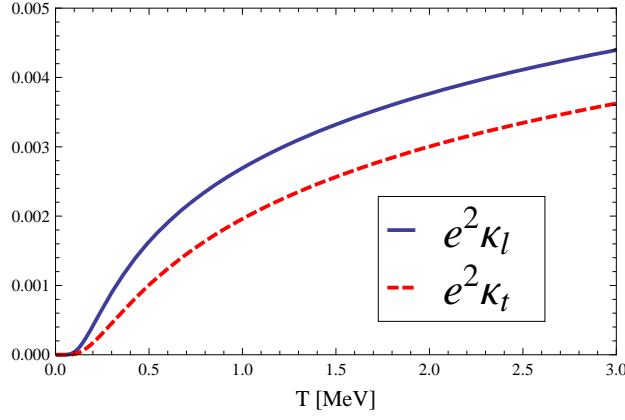


FIG. 1: The coefficients $e^2 \kappa_\ell$ and $e^2 \kappa_t$ at one loop in QED, with the fermion mass set to $m_e = 0.511 \text{ MeV}$ and $e^2 = 4\pi/137$.

In QED at leading order, the vacuum polarization reads (see for instance [14])

$$\Pi^{\text{vac}}(q^2) - \Pi^{\text{vac}}(0) = \frac{1}{2\pi^2} \int_0^1 dx x(1-x) \log \left[1 + \frac{q^2 x(1-x)}{m^2} \right]. \quad (29)$$

Two independent components of the thermal contribution read [15], with $E_{\mathbf{k}} = \sqrt{\mathbf{k}^2 + m^2}$ and $n_F(E) = 1/(e^{\beta E} + 1)$,

$$\Pi_{00}^{\text{mat}}(q) = \frac{2}{\pi^2} \text{Re} \int_0^\infty k^2 dk \frac{n_F(E_{\mathbf{k}})}{E_{\mathbf{k}}} \left[1 + \frac{4E_{\mathbf{k}}^2 - 4iE_{\mathbf{k}}q_0 - q_0^2 - \mathbf{q}^2}{4k|\mathbf{q}|} \log \frac{R_+}{R_-} \right], \quad (30)$$

$$\Pi_{\mu\mu}^{\text{mat}}(q) = \frac{4}{\pi^2} \text{Re} \int_0^\infty k^2 dk \frac{n_F(E_{\mathbf{k}})}{E_{\mathbf{k}}} \left[1 + \frac{2m^2 - q_0^2 - \mathbf{q}^2}{4|\mathbf{q}|k} \log \frac{R_+}{R_-} \right], \quad (31)$$

$$R_\pm = q_0^2 + \mathbf{q}^2 \pm 2|\mathbf{q}|k + 2iq_0 E_{\mathbf{k}}.$$

From here one obtains the longitudinal and transverse part of the polarization tensor via

$$\Pi_L(q_0^2, \mathbf{q}^2) = -\Pi_{00}(q), \quad \Pi_T(q_0^2, \mathbf{q}^2) = \frac{1}{2} (\Pi_{00}(q) - \Pi_{\mu\mu}(q)). \quad (32)$$

The expression for the fermion number susceptibility reads

$$\Pi_{00}^{\text{mat}}(q=0) = -\Pi_L(0,0) = -\Pi_L^{\text{mat}}(0,0) = \chi_s = \frac{2}{\pi^2} \int_0^\infty \frac{dk}{E_{\mathbf{k}}} n_F(E_{\mathbf{k}}) (k^2 + E_{\mathbf{k}}^2) = -\frac{2m^2}{\pi^2} \sum_{n \geq 1} (-1)^n K_2(n\beta m). \quad (33)$$

In the massless limit, we have $\chi_s = T^2/3$.

In the transverse channel, we obtain from (30–31)

$$\kappa_t = \frac{1}{3\pi^2} \int_0^\infty \frac{dk}{E_{\mathbf{k}}} n_F(E_{\mathbf{k}}) = -\frac{1}{3\pi^2} \sum_{n=1}^\infty (-1)^n K_0(n\beta m). \quad (34)$$

For small βm , we find the expansion (see appendix A)

$$\kappa_t = \frac{1}{6\pi^2} (\log(1/b) - \gamma_E) + O(b^2 \log(1/b)), \quad b \equiv \frac{m}{\pi T}. \quad (35)$$

There is an infrared divergence coming from the $T = 0$ contribution. In QCD, this divergence is driven by the light pions rather than by the light quarks, but the infrared sensitivity is also present.

It is convenient to consider the difference $\kappa_\ell - \kappa_t$, since it is infrared safe, unlike κ_ℓ and κ_t individually. We find

$$\kappa_\ell - \kappa_t = -\frac{1}{6\pi^2} \int_0^\infty dp n'_F(E_p) = -\frac{\beta m}{6\pi^2} \sum_{n=1}^\infty (-1)^n n K_1(n\beta m), \quad (36)$$

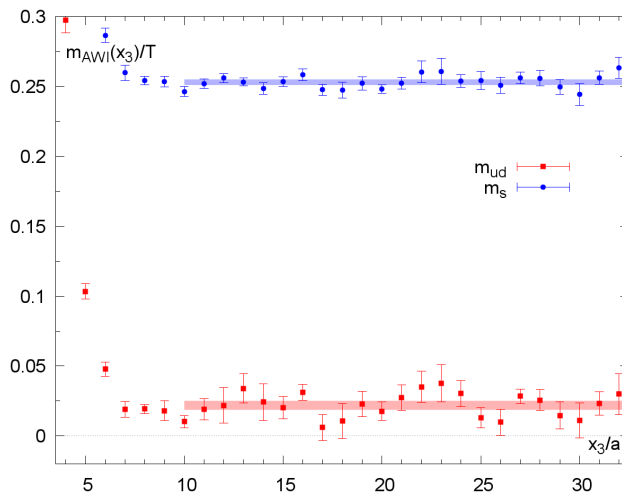


FIG. 2: The PCAC quark masses in the x_3 direction as calculated on our finite temperature lattice ensemble of size 16×64^3 . See the text for details on obtaining the quoted values m/T .

where $n'_F(E) \equiv \frac{dn_F}{dE}$. At small βm , its expansion is

$$\kappa_\ell - \kappa_t = \frac{1}{12\pi^2} \left(1 - \frac{7}{4}\zeta_3 b^2 + \frac{93}{32}\zeta_5 b^4 + \mathcal{O}(b^6) \right), \quad (37)$$

and it would not be difficult to extend the series to higher orders. Note that $\kappa_\ell - \kappa_t$ amounts to a small number compared to the fermionic contribution to the entropy, $s/T^3 = 7\pi^2/45$ in the massless case.

Finally, as a numerical application, we display the value of the coefficients κ_ℓ and κ_t in QED as a function of the temperature in Fig. 1. If we think about the early universe, we note that around the time when free neutrons start to disappear by β decay ($T \simeq 0.8\text{MeV}$, see for instance the recent review [16]), κ_ℓ and κ_t represent a 2–3 permille effect on the inter-proton electromagnetic force. By the time the nucleosynthesis chain starts (around $T = 0.1\text{MeV}$), the effect really is tiny.

If we now consider the quark-gluon plasma, we expect the difference $\kappa_\ell - \kappa_t$ to be well described by the leading perturbative formulae above (with the suitable N_c and N_f factors) at sufficiently high temperature, since it is not infrared-sensitive at leading order in perturbation theory. The value of the individual coefficients κ_ℓ and κ_t however emerge from an interesting interplay between ultraviolet and infrared physics. Indeed, without the vacuum subtraction, they would be ultraviolet divergent, but on the other hand, the vacuum contribution is infrared divergent for massless fermions. In QCD, this infrared contribution is non-perturbative (it is dominated by pions), and therefore we turn to lattice simulations in order to evaluate κ_ℓ and κ_t individually.

III. NUMERICS

In this section, we describe a numerical lattice QCD calculation of the antiscreening coefficients κ_l and κ_t , as well as of the free energy of two static leptons for a general separation r .

All our numerical results were obtained on dynamical gauge configurations with two mass-degenerate quark flavors. The gauge action is the standard Wilson plaquette action [17], while the fermions were implemented via the $\mathcal{O}(a)$ improved Wilson discretization with non-perturbatively determined clover coefficient c_{sw} [18]. The configurations were generated using the MP-HMC algorithm [19, 20] in the implementation of Marinkovic and Schaefer [21] based on Lüscher's DD-HMC package [22].

We calculated correlation functions using the same discretization and masses as in the sea sector on two lattice ensembles. One at zero temperature and a lattice of size 128×64^3 (labeled O7 in [23]) with a lattice spacing of $a = 0.0486(4)(5)\text{fm}$ [23] and a pion mass of $m_\pi = 270\text{MeV}$, so that $m_\pi L = 4.2$. The second at finite temperature with a lattice of size 16×64^3 with all bare parameters identical to the zero-temperature ensemble. The zero-temperature ensemble was made available to us through the CLS effort [24], while the second ensemble was generated by us and already presented in [5]. Note that choosing $N_\tau = 16$ yields a temperature of $T \simeq 250\text{MeV}$. Based on preliminary

$6/g_0^2$	5.50
κ	0.13671
c_{SW}	1.751496
m_π [MeV]	270
Z_V	0.768(5)
a [fm]	0.0486(4)(5)
$T_{N_\tau=16}$ [MeV]	253(4)
$\overline{m}_{ud}^{\overline{MS}}(2 \text{ GeV})/T$	0.0325(48)(7)
$\overline{m}_s^{\overline{MS}}(2 \text{ GeV})/T$	0.3747(30)(86)

TABLE I: The top block shows the bare lattice parameters, for more details on the $N_\tau = 128$ and $N_\tau = 16$ ensembles see [5, 23, 25]. The middle block summarizes the pion mass, the vector renormalization constant [33], the lattice spacing [23] and the corresponding temperature of our $N_\tau = 16$ lattice calculation. In the bottom block we give the renormalized quark masses in units of temperature, where the first error is from the bare axial Ward identity mass and the second from the renormalization factor.

results on the pseudo-critical temperature T_c of the crossover from the hadronic to the high-temperature phase [25], the temperature can also be expressed as $T/T_c \approx 1.2$.

In addition we calculated correlation functions on the same ensembles with the bare quark mass tuned to match the physical strange quark mass [26]. More precisely, the bare quark mass is fixed at zero temperature by tuning the kaon mass to the value realized in nature. According to perturbation theory, the most relevant dimensionless parameter is m/T . In order to facilitate a comparison with the one-loop results, we therefore measure this quantity directly using the partially conserved axial current (PCAC) relation [27, 28] in the finite-temperature ensemble. Since it is an operator identity, we are free to evaluate the correlation functions of the axial current and the pseudoscalar density in the longer spatial direction to evaluate the quark mass. Specifically, we define

$$m_{\text{AWI}}(x_3) = \frac{1}{2} \sum_{(x_0, x_1, x_2)} \frac{\langle \partial_3^{\text{imp}} J_{3,5}^I(x) J_5(0) \rangle}{\langle J_5(x_i) J_5(0) \rangle}, \quad (38)$$

where $J_5(x_i)$ and $J_{\mu,5}^I(x_i) = J_{\mu,5}(x_i) + ac_A \partial_\mu^{\text{imp}} J_5(x_i)$ denote the (isovector) pseudoscalar density and improved axial-vector current, respectively. As ‘improved’ lattice derivatives $\partial_\mu^{\text{imp}}$ we use the higher-order difference scheme given in [29], Eq. (2.18–2.19). Here, for the improvement coefficient c_A we use the non-perturbatively determined value of [30]. The extraction of the PCAC mass is illustrated in Fig. 2. The quoted values for m/T were determined by fitting a constant to $m_{\text{AWI}}(x_3)$ over the interval indicated by the band in Fig. 2. The result was found to be stable under variations of the fit interval. To renormalize the PCAC quark mass we use the non-perturbatively determined renormalization factors Z_A and Z_P of the axial current and the pseudoscalar density of [23, 31], as well as the conversion factor from the Schrödinger functional scheme to the \overline{MS} scheme from [23, 32]. Altogether the factor by which we multiply the bare PCAC mass to obtain the \overline{MS} mass at a renormalization scale of $\mu = 2 \text{ GeV}$ is 1.481(34). The result as well as all relevant parameters are collected in Tab. I. From now on we simply refer to these \overline{MS} quark masses by m .

We implemented the vector correlation function as a mixed correlator between the local and the conserved current. In the following we will require the three correlation functions:

$$G^{\text{bare}}(x_0, g_0, T) \delta_{kl} = -a^3 \sum_{(x_1, x_2, x_3)} \langle J_k^c(x) J_l^\ell(0) \rangle, \quad k, l = 1, 2, 3, \quad (39)$$

$$G_t^{\text{bare}}(x_3, g_0, T) \delta_{ij} = -a^3 \sum_{(x_0, x_1, x_2)} \langle J_i^c(x) J_j^\ell(0) \rangle, \quad i, j = 1, 2, \quad (40)$$

$$G_l^{\text{bare}}(x_3, g_0, T) = -a^3 \sum_{(x_0, x_1, x_2)} \langle J_0^c(x) J_0^\ell(0) \rangle, \quad (41)$$

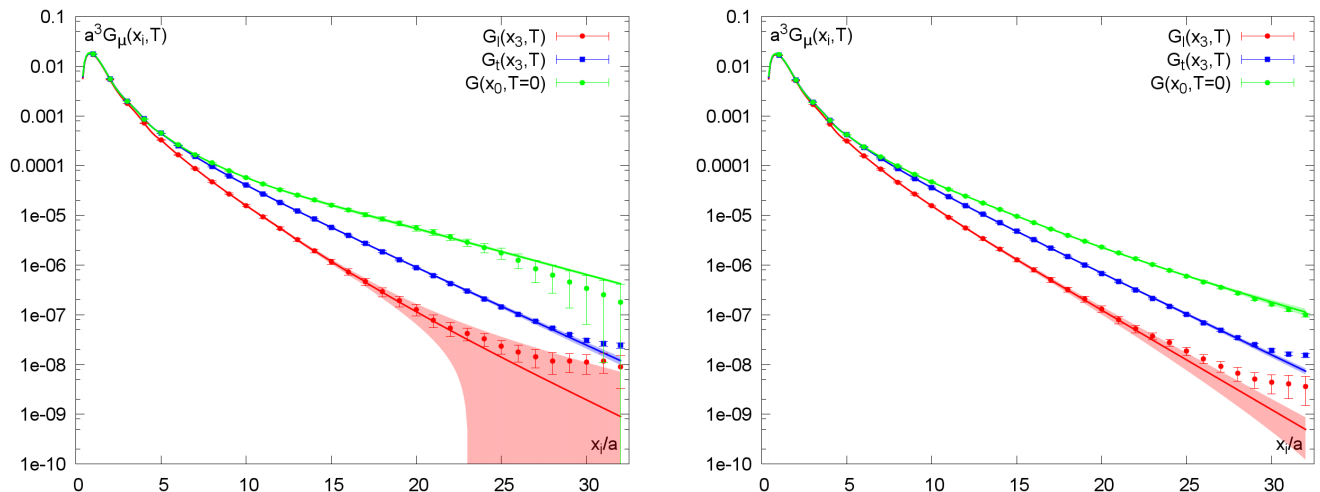


FIG. 3: Local-conserved vector correlation functions for the light quarks (left panel) and the strange quark (right panel). The shaded bands represent the correlators entering the computation of the antiscreening coefficients and the free energy.

where

$$J_\mu^l(x) = \frac{1}{\sqrt{2}} \bar{q}(x) \gamma_\mu \tau^3 q(x), \quad (42)$$

$$J_\mu^c(x) = \frac{1}{2\sqrt{2}} \left(\bar{q}(x + a\hat{\mu})(1 + \gamma_\mu) U_\mu^\dagger(x) \tau^3 q(x) - \bar{q}(x)(1 - \gamma_\mu) U_\mu(x) \tau^3 q(x + a\hat{\mu}) \right). \quad (43)$$

Here q represents a doublet of mass-degenerate quark fields and τ^3 the diagonal Pauli matrix acting on the flavor indices. The doublet can be interpreted as the (u, d) quarks (which are treated fully dynamically) for the light mass case, while it can be interpreted as a ‘partially quenched’ (s, s’) doublet for the heavier case (i.e. their back-reaction on the thermal system is neglected). We note that with this normalization of the current, the perturbative prediction for its two-point function is given by $N_c = 3$ times the expressions given in section II D.

We have renormalized the vector correlator using

$$G_\mu(x_i, T) = Z_V(g_0) G_\mu^{\text{bare}}(x_i, g_0, T) \quad (44)$$

with the non-perturbative value of $Z_V = 0.768(5)$ [33]. We have not included $O(a)$ contributions from the improvement term proportional to the derivative of the antisymmetric tensor operator [34, 35]. A quark-mass dependent improvement term of the form $(1 + b_V(g_0)am_q)$ [35] was also neglected. These contributions should eventually be included to ensure a smooth scaling behavior as the continuum limit is taken. Here, our primary goal is to carry out the analysis on a single lattice spacing.

A. Correlator data and screening masses

Reaching our goal of computing the antiscreening coefficients and the free energy requires the computation of three vector correlation functions: the vector correlator at zero temperature (Eq. 39) in the x_0 direction, as well as the individual transverse (Eq. 40) and longitudinal (Eq. 41) vector correlators in the x_3 -direction.

To treat the latter required integrals over the spatial vector correlation functions without introducing unnecessarily large finite lattice effects, we employ the position space representation introduced in [36]. Here, the local-conserved correlator was extrapolated with an exponential that decays with the lowest-lying ‘mass’ [39]. This mass can be fixed by fitting to the lattice data an Ansatz of the form

$$G_{\text{Ansatz}}(x_i) = \sum_{n=1}^2 |A_n|^2 e^{-m_n x_i}, \quad (45)$$

for x_i sufficiently below the half-lattice extent $N_i/2$ that the ‘backward’ propagating states give a negligible contribution. In the zero temperature ensemble this mass can be determined reliably by extracting it from a separate

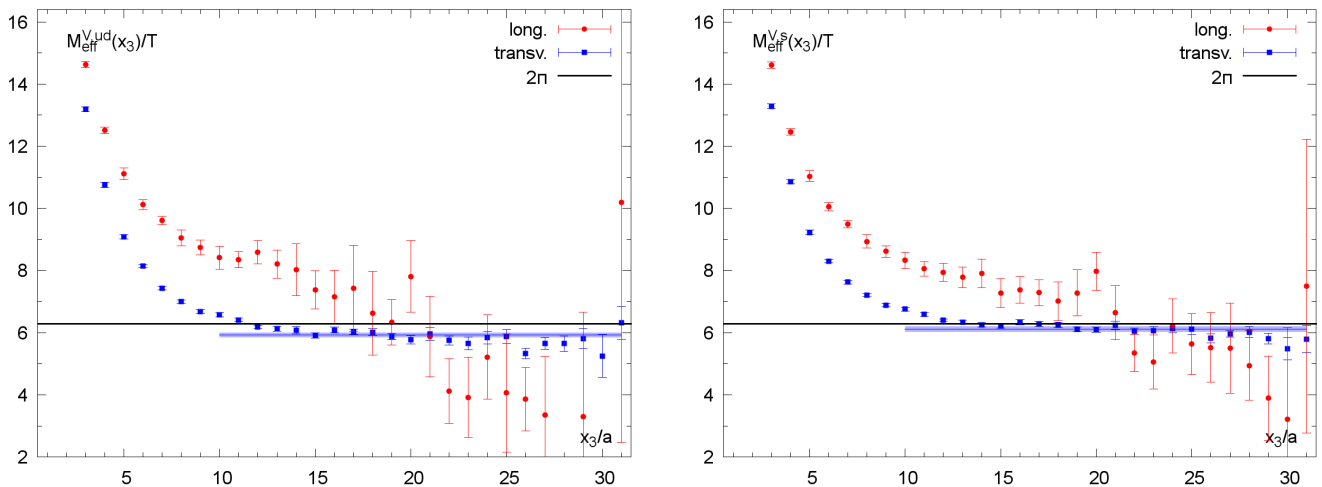


FIG. 4: The effective screening masses (defined by Eq. (46)) for the longitudinal and the transverse channels. The left panel corresponds to the light quark case and the right panel to the strange quark. The band shows the result of the fit for the mass with its statistical error.

correlation function, computed on the same configurations using smeared operators at the source and sink [26, 36]. This operator has greater overlap with the ground state and yields more precise data. The mass parameter determined in this way is then carried over to the local-conserved correlator and the corresponding prefactor of the exponential $|A_1|^2$ is fitted to the lattice data around $x_0 = \beta/4$. For the finite temperature ensembles, we did not compute vector correlation functions using smeared-smeared operators but fitted using the local-conserved data directly. However, due to the better signal-to-noise ratio in the finite temperature case, accurate results can nevertheless be obtained in this fashion.

The raw lattice data as well as the resulting correlation functions are shown as the colored shaded bands in Fig. 3, where the error estimates were obtained via a jackknife procedure. For the light-quark longitudinal correlator, the relative errors grow rapidly for $x_3/a \gtrsim 20$, but this has little impact on our determination of the antiscreening coefficients and the free energy of two static leptons.

As a byproduct of our study, we can investigate the lowest-lying screening masses coupling to the isovector vector current. For that purpose, in Fig. 4 we display the effective screening masses, defined by the implicit equation

$$\frac{G(x_3 - a/2)}{G(x_3 + a/2)} = \frac{\cosh [M_{\text{eff}}^V(x_3)(L/2 - (x_3 - a/2))]}{\cosh [M_{\text{eff}}^V(x_3)(L/2 - (x_3 + a/2))]} \quad (46)$$

This form corrects for the leading effects of the finite length of the x_3 direction. In the transverse channel, we observe a convincing plateau, showing that we observe the asymptotic screening mass. In the longitudinal channel, the correlator initially falls off with a substantially higher exponent, but at distances beyond $x_3 \approx \beta$, the effective exponent appears to decrease to a value below $2\pi T$. A possible interpretation is that the charge density operator couples only weakly to the lightest state in that channel, and therefore initially decays with a higher exponent. Given this behavior, we leave the extraction of a screening mass in the longitudinal channel for a future study with increased statistics and possibly improved spectroscopic methods. In the transverse channel, we extract the following values for the screening mass,

$$\frac{M_t^V}{2\pi T} = \begin{cases} 0.943(17) & \text{light quarks} \\ 0.973(21) & \text{strange quarks.} \end{cases} \quad (47)$$

The quoted error contains an estimate of the uncertainty associated with choosing a fit interval. We thus have rather convincing evidence that the screening mass lies below $2\pi T$ for light quarks. These results can be compared to the perturbative prediction $M_t^V/(2\pi T) = 1 + 0.02980g^2$ for two massless flavors of quarks [37]. Presumably the value of the screening mass reaches values above $2\pi T$ at sufficiently high temperatures. Interestingly, the charge density operator (corresponding to the longitudinal channel) also plays a somewhat special role in the perturbative analysis [37]. It would be worth revisiting this special case. In addition to the masses, the coupling $|A_1|^2$ of the lightest screening state to the vector current is of significant interest. In the regime where the hierarchy $gT \ll \pi T$ applies, it is proportional

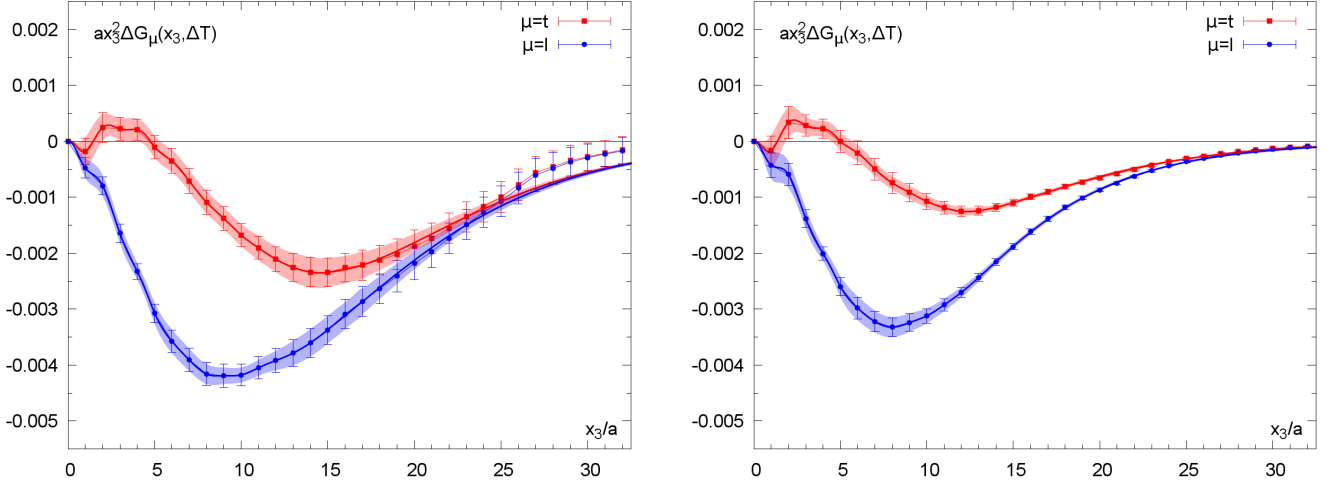


FIG. 5: The integrands $x_3^2 \Delta G_\mu(x_3, T)$ for the convolution integrals of Eq. (49) and Eq. (50) for the light quark mass m_{ud} in the left panel and the strange quark mass m_s in the right panel.

to the wavefunction at the origin describing the bound state of two fermions effectively of mass πT . We find, in the transverse channel,

$$\frac{1}{T^3} |A_1|^2 = \begin{cases} 6.05 \pm 0.78 & \text{light quarks} \\ 5.80 \pm 1.10 & \text{strange quarks.} \end{cases} \quad (48)$$

A future comparison with perturbative calculations would be complementary to the comparison of the screening masses.

B. The antiscreening coefficients κ_t , κ_l and $(\kappa_l - \kappa_t)$

In order to obtain κ_t , κ_l and $(\kappa_l - \kappa_t)$ given the local-conserved correlation functions of Fig. 3, one has to compute the following integrals:

$$\kappa_t = - \int_0^\infty dx x^2 \Delta G_t(x, T), \quad \Delta G_t(x, T) \equiv G_t(x, T) - G(x, 0), \quad (49)$$

$$\kappa_l = - \int_0^\infty dx x^2 \Delta G_l(x, T), \quad \Delta G_l(x, T) \equiv G_l(x, T) - G(x, 0), \quad (50)$$

$$\kappa_l - \kappa_t = - \int_0^\infty dx x^2 \Delta G_{l-t}(x, T), \quad \Delta G_{l-t}(x, T) \equiv G_l(x, T) - G_t(x, T). \quad (51)$$

To compute these integrals, we employ the parametrized correlation functions of Fig. 3, form the relevant differences, multiply the latter by x^2 and integrate them. The integrands for κ_t and κ_l in the light quark case are shown in the left panel of Fig. 5, while the corresponding strange quark results are given in the right panel. At large distances, $x_3 \gtrsim 2/T$, the integrand is strongly suppressed. At the same time, the explicit factor x_3^2 induces an exact zero at $x_3 = 0$ in the integrand. For the longitudinal case a broad peak in the negative y -direction emerges with a minimum at $x_3 \simeq (2T)^{-1}$. In the transverse case the integrand first yields positive results before passing through zero and also exhibiting a negative peak shape. Both results depend strongly on the mass value, as the light-quark curve drops roughly a factor 1.5–2.0 lower than the strange-quark curve.

The integral is carried out using standard numerical integration techniques (for example the ‘global adaptive’ strategy using the ‘Gauss-Kronrod rule’ or ‘trapezoidal rule’ options supplied by the Mathematica-package work very well here) for a set of jackknife bins, yielding a central value and an error estimate. We obtain, for the two quark masses,

$$\kappa_t(m_{\text{ud}}) = 0.0400(39), \quad \kappa_t(m_s) = 0.0169(17), \quad (52)$$

$$\kappa_l(m_{\text{ud}}) = 0.0750(34), \quad \kappa_l(m_s) = 0.0458(19). \quad (53)$$

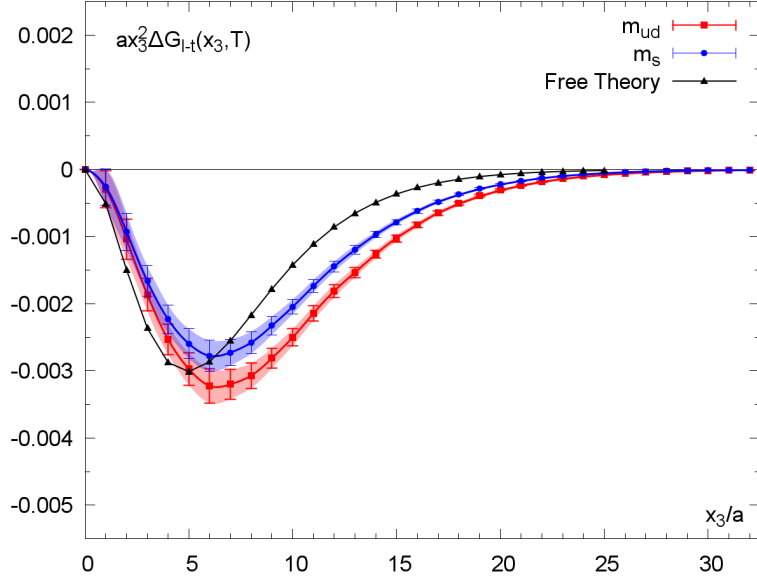


FIG. 6: The integrand $x_3^2 \Delta G_{l-t}(x_3, T)$ of Eq. (51) for the light and the strange quark cases. The corresponding quantity for free massless fermions is displayed as a black curve.

These values are similar to the corresponding one-loop QED predictions for $m/T \simeq 1$ (if one divides the former by the $N_c = 3$ factor). This reflects the fact that the infrared behavior of the vector correlator in QCD is very different from its QED counterpart due to confinement and chiral symmetry breaking. In QED, a substantial fermion mass mimicks to a certain extent the rapid fall-off of the QCD correlator.

Since the zero temperature correlator drops out in $(\kappa_l - \kappa_t)$, the latter difference is determined more accurately. The corresponding integrand for both masses is shown in Fig. 6, where we also give the one-loop lattice result (computed in appendix B) for comparison. For both values of the quark mass we observe a broad peak in the negative direction. While qualitatively similar, the non-perturbative data falls off somewhat more slowly than the one-loop result, in spite of the fact that the quark mass is finite in the simulation and set to zero in the one-loop curve. The resulting values of the integrals are:

$$(\kappa_l - \kappa_t)(m_{ud}) = 0.0350(24), \quad (\kappa_l - \kappa_t)(m_s) = 0.0290(21). \quad (54)$$

Due to the slower fall-off of the screening correlators observed in the data, the value of this difference is noticeably larger than the one-loop calculation predicts,

$$(\kappa_l - \kappa_t)_{m/T=0.033} = 0.0253, \quad (\kappa_l - \kappa_t)_{m/T=0.38} = 0.0246 \quad (\text{one loop}), \quad (55)$$

particularly for the light quark mass case. It would be interesting to see whether a two-loop calculation could account for the discrepancy.

C. Implications for the free energy of two static leptons in the quark-gluon plasma

To compute the free energy of two static electric charges in a QCD plasma in the one-photon exchange approximation, it is useful to switch to a position-space representation of the one-loop correction to the static photon propagator. The reason is that the integral over the module of the spatial momentum in Eq. (20) is not absolutely convergent. Defining $\tilde{j}_\mu(x_3) \equiv \int dx_0 dx_1 dx_2 j_\mu(x)$, the representation

$$F_l^{(2)}(r, T) = \frac{Q_1 Q_2 e^2 e^{-m_e r}}{4\pi r} \left(1 + e^2 h_l(r, T) \right), \quad (56)$$

$$h_l(r, T) = \int_0^\infty dx_3 \left(\phi_\ell(r, x_3) \langle \tilde{j}_0(x_3) j_0(0) \rangle_T - x_3^2 \langle \tilde{j}_0(x_3) j_0(0) \rangle_0 \right), \quad (57)$$

$$\phi_\ell(r, x_3) = \begin{cases} x_3^2 & x_3 < r, \\ 2x_3 r - r^2 & x_3 \geq r, \end{cases} \quad (58)$$

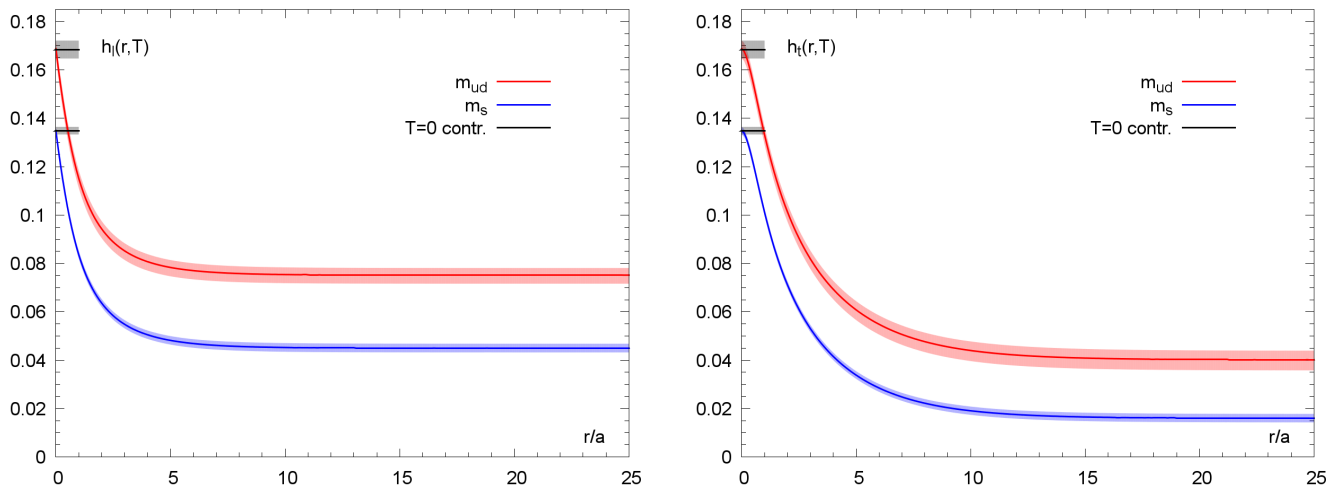


FIG. 7: The modification terms of the free energy of two static charges in a QED plasma. Left: $h_l(r, T)$ of Eq. (56). Right: $h_t(r, T)$ of Eq. (59). In both cases the light and strange quark results are displayed respectively in red and blue. We highlight the r -independent $T = 0$ contribution in black around $r = 0$.

is equivalent, up to higher order terms in the coupling e , to Eq. (20). However, the integral over x_3 to be performed numerically is now exponentially convergent for all r in the infrared, and the integrand is finite around $x_3 = 0$. Moreover, since we identified the exponential fall-off of the correlator at long distances, this representation is less affected by the finite box length L_3 used in the simulation [36] than the momentum space representation.

We recall that in the continuum, the two integrals contributing to h_l taken separately are logarithmically divergent in the ultraviolet, but that their difference is finite. On the lattice, the corresponding sums are of course separately finite. For large r , $h_l(r, T)$ tends to κ_l . For small r , the thermal correlator can be approximated by the vacuum correlator and one recovers from Eq. (56) the standard expression for the potential $V(\mathbf{r})$ modified by vacuum polarization effects, the so-called Uehling potential (see for instance [14]).

Similarly, in the case of two stationary, parallel currents, the negative derivative of the free energy reads

$$-\frac{1}{L_3} \frac{\partial}{\partial r} F_t^{(2)}(r, T) = -\frac{I_1 I_2 e^2}{2\pi r} \left(1 + e^2 h_t(r, T)\right), \quad (59)$$

$$h_t(r, T) = \int_0^\infty dx_3 \left(\phi_t(r, x_3) \langle \tilde{j}_1(x_3) j_1(0) \rangle_T - x_3^2 \langle \tilde{j}_1(x_3) j_1(0) \rangle_0 \right), \quad (60)$$

$$\phi_t(r, x_3) = \begin{cases} x_3^2 & x_3 < r, \\ x_3^2 - x_3 \sqrt{x_3^2 - r^2} - r^2 \log \frac{r}{x_3 + \sqrt{x_3^2 - r^2}} & x_3 \geq r. \end{cases} \quad (61)$$

These equations allow us to compute the generalization of the electric Ampère force for currents immersed in hot, strongly interacting matter.

Now the integrals in Eq. (56) and Eq. (59) are of the same form as those of Eqs. (49–51) and to compute these loop corrections we may reuse the machinery developed to calculate the antiscreening coefficients. The results for both correction functions are shown in Fig. 7, where the red and blue lines denote the light and strange quark mass cases, respectively. We give the distance r in lattice units and highlight the r -independent $T = 0$ contribution by short black bands around $r = 0$ (again, this contribution is logarithmically divergent in the continuum limit). In both cases we observe a sharp drop from the $T = 0$ contribution at small r with the results leveling off to a constant. In the case of the free energy of two static leptons in the left panel of Fig. 7, the dependence on r rapidly becomes negligible; it levels off into a constant shift to the leading order term at around $r/a \simeq 10$. At this point the results for the two masses differ by roughly a factor 1.5. In the case of the derivative of the free energy of two parallel currents, the distance dependence quickly becomes negligible and levels off around $r/a \simeq 20$. In this case the mass dependence is seen to give roughly a factor 2 between the light and strange quark cases. Comparing the errors from the $T = 0$ contribution and the respective $T \neq 0$ parts, we note that the $T = 0$ uncertainty dominates at large distances. In the limit $r \rightarrow \infty$ the terms $h_l(r, T)$ and $h_t(r, T)$ become equivalent to those of Eq. (49) and Eq. (50), which provides a useful cross-check of our calculations and indeed the results agree as expected.

To illustrate the difference of this result with the zero-temperature case, we display the hadronic vacuum polarization

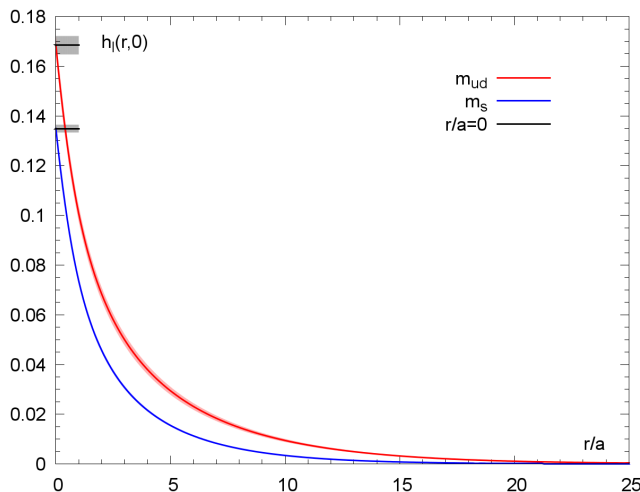


FIG. 8: The hadronic vacuum polarization contribution $h_l(r,0)$ to the potential between two electric charges. Note that $r/a = 20$ corresponds roughly to $r = 1\text{fm}$.

contribution to the electric potential between two electric charges in Fig. 8. In the limit $T \rightarrow 0$, Eq. (56) simplifies to

$$V(r) = \frac{Q_1 Q_2 e^2}{4\pi r} \left(1 + e^2 h_l(r,0) \right), \quad (62)$$

$$h_l(r,0) = - \int_r^\infty dx_3 (r - x_3)^2 \langle \tilde{j}_0(x_3) j_0(0) \rangle_0. \quad (63)$$

In particular, the relative correction $h(r,0)$ to the Coulomb potential is positive definite, i.e. the effective QED coupling becomes stronger at short distances, as expected. Unlike in the thermal case, the correction goes to zero rapidly beyond a distance of 1fm.

IV. CONCLUSION

We have studied two static properties of quantum relativistic plasmas. They represent a loop correction to the free energy of external static charges and stationary currents, where charge renormalization has been performed. In a hydrodynamic treatment, κ_t enters the constitutive equation of the current and thus governs the linear response to an external magnetic field with a non-vanishing curl. We have calculated these two coefficients at one-loop order in perturbation theory for QED and using lattice QCD for the non-Abelian case. Remarkably, the presence of the plasma generates an antiscreening of electric currents and thereby an enhancement of the Ampère force between two currents. Our emphasis has been on the interpretation of these quantities and on the best suited strategies to compute them; in order to make a realistic prediction for QCD it would be necessary to explore the quark mass dependence and to take the continuum limit of the coefficients $\kappa_{l,t}$. While it appears unlikely that these physical effects have any observable consequence in primordial nucleosynthesis, it would be interesting to investigate further whether the coefficient κ_t has any observable consequences, be it in the QED or in the QCD plasma.

Acknowledgments

We are grateful for the access to the zero-temperature ensemble used here, made available to us through CLS. We also warmly thank Georg von Hippel who provided the smeared vector correlator on this ensemble. We acknowledge the use of computing time for the generation of the gauge configurations on the JUGENE computer of the Gauss Centre for Supercomputing located at Forschungszentrum Jülich, Germany; the finite-temperature ensemble was generated within the John von Neumann Institute for Computing (NIC) project HMZ21. The correlation functions were computed on the dedicated QCD platform “Wilson” at the Institute for Nuclear Physics, University of Mainz. This work was supported by the *Center for Computational Sciences in Mainz* as part of the Rhineland-Palatinate Research Initiative and by the DFG grant ME 3622/2-1 *Static and dynamic properties of QCD at finite temperature*.

Appendix A: Treelevel calculation of κ_ℓ and κ_t

With $\tilde{j}_1(x_3) = \int dx_0 dx_1 dx_2 j_1(x)$, the coefficient κ_t can be computed as follows,

$$\kappa_t = -\frac{\partial}{\partial(q_3^2)} \int_{-\infty}^{\infty} dx_3 \langle \tilde{j}_1(x_3) j_1(0) \rangle \Big|_0^T e^{iq_3 x_3} \Big|_{q_3=0} = +\frac{1}{2} \int_{-\infty}^{\infty} dx_3 x_3^2 \langle \tilde{j}_1(x) j_1(0) \rangle \Big|_0^T. \quad (\text{A1})$$

Using the spectral representation of the screening correlator,

$$-\langle \tilde{j}_1(x_3) j_1(0) \rangle = \int_0^\infty \frac{d\omega}{2\pi} \tilde{\rho}_{11}(\omega, T) e^{-\omega|x_3|}, \quad (\text{A2})$$

we obtain the expression

$$\kappa_t = -\frac{1}{\pi} \int_0^\infty \frac{d\omega}{\omega^3} (\tilde{\rho}_{11}(\omega, T) - \omega^2 \rho^{\text{vac}}(\omega^2)). \quad (\text{A3})$$

Introducing the notation

$$p_n^\pm = (2n \pm 1)\pi T, \quad E_n^\pm = (p_n^{\pm 2} + m^2)^{1/2}, \quad (\text{A4})$$

the spectral functions are given by, for $\omega \geq 0$,

$$\rho^{\text{vac}}(\omega^2) = \frac{1}{6\pi} \sqrt{1 - 4m^2/\omega^2} (1 + 2m^2/\omega^2) \theta(\omega - 2m), \quad (\text{A5})$$

$$\tilde{\rho}_{11}(\omega, T) = \frac{\omega}{2\beta} \sum_{n=1}^{\infty} \left(1 + (2E_n^-/\omega)^2\right) \theta(\omega - 2E_n^-). \quad (\text{A6})$$

We consider different intervals of frequency separately. From the low-frequency region, we get a purely vacuum contribution,

$$\kappa^{\text{low}} = \frac{1}{\pi} \int_0^{2E_0^+} \frac{d\omega}{\omega} \rho^{\text{vac}}(\omega^2) = \frac{1}{36\pi^2} \left(6 \operatorname{asinh}(\pi/(\beta m)) - \frac{\pi(6\beta^2 m^2 + 5\pi^2)}{(\beta^2 m^2 + \pi^2)^{3/2}}\right) \quad (\text{A7})$$

If we define $\tilde{\rho}_{11}(\omega, n, T)$ for $n \geq 1$ such that

$$\tilde{\rho}_{11}(\omega, n, T) = \tilde{\rho}_{11}(\omega, T) \quad \text{for} \quad 2E_n^- \leq \omega \leq 2E_n^+, \quad (\text{A8})$$

one finds

$$\tilde{\rho}_{11}(\omega, n, T) = \frac{n}{6\beta^3 \omega} (3\beta^2(\omega^2 + 4m^2) + 4\pi^2(4n^2 - 1)). \quad (\text{A9})$$

Thus the coefficient κ_t is given by

$$\kappa_t = \kappa^{\text{low}} + \sum_{n=1}^{\infty} g_b(\beta, n), \quad (\text{A10})$$

$$g_b(\beta, n) \equiv -\frac{1}{\pi} \int_{2E_n^-}^{2E_n^+} \frac{d\omega}{\omega^3} (\tilde{\rho}_{11}(\omega, n, T) - \omega^2 \rho^{\text{vac}}(\omega^2)) \quad (\text{A11})$$

The summand $g_b(\beta, n)$ is easily obtained analytically but the expression is not very illuminating and we do not reproduce it here. The series is absolutely convergent. Moreover, $g_b(\beta, n)$ can be expanded in positive powers of β , and each term in the expansion is an absolutely convergent series in n . The small βm expansion is thus straightforwardly obtained in this way. Note that the infrared divergence in κ_t when $m \rightarrow 0$ comes entirely from κ^{low} .

For κ_ℓ , the calculation proceeds in the same way,

$$\kappa_\ell = -\frac{1}{\pi} \int_0^\infty \frac{d\omega}{\omega^3} (\tilde{\rho}_{00}(\omega, T) - \omega^2 \rho^{\text{vac}}(\omega^2)), \quad (\text{A12})$$

with the relevant screening spectral function given by

$$\tilde{\rho}_{00}(\omega, T) = \frac{\omega}{\beta} \sum_{n=1}^{\infty} (1 - (2p_n^-/\omega)^2) \theta(\omega - 2E_n^-). \quad (\text{A13})$$

We then have

$$\tilde{\rho}_{00}(\omega, T) = \tilde{\rho}_{00}(\omega, n, T) \equiv \frac{n\omega}{\beta} + \frac{4\pi^2 n(1 - 4n^2)}{3\beta^3 \omega}, \quad 2E_n^- < \omega < 2E_n^+. \quad (\text{A14})$$

Defining $g_\ell(\beta, n)$ analogously to $g_b(\beta, n)$ with $\tilde{\rho}_{11}$ replaced by $\tilde{\rho}_{00}$, we have $\kappa_\ell = \kappa^{\text{low}} + \sum_{n=1}^{\infty} g_\ell(\beta, n)$. The expansion (36) for $\kappa_\ell - \kappa_t = \sum_{n=1}^{\infty} [g_\ell(\beta, n) - g_b(\beta, n)]$, is obtained from

$$g_\ell(\beta, n) - g_b(\beta, n) = \frac{(p_n^+ + p_n^-)(E_n^+ - E_n^-)}{48\pi^2 (E_n^- E_n^+)^3} \left[(m^2 + p_n^+ p_n^-) (E_n^{+2} + E_n^+ E_n^- + E_n^{-2}) - 3E_n^{-2} E_n^{+2} \right]. \quad (\text{A15})$$

This expression can be expanded in positive powers of β , and then the individual Taylor coefficients can be summed over n . The series in n are all absolutely convergent.

In order to obtain a representation more suitable for large values of βm , one uses the Poisson summation formula to rewrite the screening correlators

$$-\langle \tilde{j}_\mu(x_3) j_\mu(0) \rangle = 2 \sum_{j \in \mathbb{Z}} (-1)^j \int \frac{d^3 \mathbf{p}}{(2\pi)^3} \frac{e^{-2E_{\mathbf{p}} |x_3| + i p_3 \beta j}}{E_{\mathbf{p}}^2} (E_{\mathbf{p}}^2 - p_\mu^2), \quad (\text{no summation over } \mu; \mu \neq 3). \quad (\text{A16})$$

In particular one obtains $\kappa_\ell - \kappa_t$ by integrating the difference of the two correlators over x_3 ,

$$\kappa_\ell - \kappa_t = \int_0^\infty dx_3 x_3^2 \langle \tilde{j}_0(x_3) j_0(0) - \tilde{j}_1(x_3) j_1(0) \rangle \quad (\text{A17})$$

$$= -\frac{1}{8\pi^2} \sum_{j \in \mathbb{Z} \setminus \{0\}} (-1)^j \int_0^\infty \frac{p dp}{E_p^5} \left(p^2 + 3 \frac{\partial^2}{j^2 \partial \beta^2} \right) \frac{\sin(p\beta j)}{\beta j}. \quad (\text{A18})$$

Note that the term $j = 0$ does not contribute, because it corresponds to the $T = 0$ situation, where by rotation invariance the two correlators are equal. The integrals are now linear combinations of modified Bessel functions and we arrive at Eq. (36).

Appendix B: Lattice perturbation theory

We consider a fermion described by the Wilson action. Defining

$$\hat{p}_\mu = \frac{2}{a} \sin \frac{ap_\mu}{2}, \quad \hat{p}_\mu^\circ = \frac{1}{a} \sin ap_\mu, \quad M_p = \frac{1}{2} a \hat{p}^2 + m, \quad (\text{B1})$$

$$\int_p f(p) \equiv \frac{1}{\beta} \sum_{n_0=1}^{\beta/a} \int_{-\pi/a}^{\pi/a} \frac{d^3 \mathbf{p}}{(2\pi)^3} f((2n_0 - 1)\pi/\beta, \mathbf{p}), \quad (\text{B2})$$

the propagator reads

$$G_w(x, y) \equiv \langle \psi(x) \bar{\psi}(y) \rangle = \int_p \frac{e^{ip(x-y)}}{i\gamma_\mu \hat{p}_\mu^\circ + M_p}. \quad (\text{B3})$$

Consider the local vector current $\bar{\psi}(x) \gamma_\mu \psi(x)$ and the conserved vector current

$$V_\mu(x) = \frac{1}{2} (\bar{\psi}(x + a\hat{\mu})(1 + \gamma_\mu) U_\mu^\dagger(x) \psi(x) - \bar{\psi}(x)(1 - \gamma_\mu) U_\mu(x) \psi(x + a\hat{\mu})). \quad (\text{B4})$$

Its correlation function with the local current is

$$\begin{aligned} G_{\mu\nu}^{\text{CL}}(x) &\equiv -\langle V_\mu(x) \bar{\psi}(0) \gamma_\nu \psi(0) \rangle \\ &= \frac{1}{2} \text{Tr} \{ (1 + \gamma_\mu) G(x, 0) \gamma_\nu G(0, x + a\hat{\mu}) - (1 - \gamma_\mu) G(x + a\hat{\mu}) \gamma_\nu G(0, x) \}. \end{aligned} \quad (\text{B5})$$

Inserting expression (B3) for the fermion propagator and performing the Dirac traces, we obtain

$$\begin{aligned}
a^4 \sum_x G_{\mu\nu}^{\text{CL}}(x) e^{ik(x+a\hat{\mu}/2)} &\equiv -\Pi_{\mu\nu}^{\text{CL}}(k) \\
&= 4 \int_p \frac{\cos[a(p_\mu + \frac{k_\mu}{2})](\delta_{\mu\nu}(\hat{p} \cdot \hat{q} + M_p M_q) - \hat{p}_\mu \hat{q}_\nu - \hat{p}_\nu \hat{q}_\mu) - \sin[a(p_\mu + \frac{k_\mu}{2})](M_p \hat{q}_\nu + M_q \hat{p}_\nu)}{(\hat{p}^2 + M_p^2)(\hat{q}^2 + M_q^2)} \Big|_{q=p+k}.
\end{aligned} \tag{B6}$$

The correlator satisfies

$$\sum_\mu \hat{k}_\mu \Pi_{\mu\nu}^{\text{CL}}(k) = 0. \tag{B7}$$

Another representation is, on a spatial torus with infinite time extent,

$$a^3 \sum_x G_{11}^{\text{CL}}(x) \stackrel{x_0 \neq 0}{=} \frac{4}{L_1 L_2 L_3} \sum_p \frac{e^{-2\omega_p |x_0|}}{D(\mathbf{p})^2} \left[\cos(ap_1) \left(D(\mathbf{p})^2 / (2A(\mathbf{p}))^2 + \hat{\mathbf{p}}^2 - 2\hat{p}_1^2 + C(\mathbf{p})^2 \right) - 2a\hat{p}_1^2 C(\mathbf{p}) \right], \tag{B8}$$

$$a^3 \sum_x G_{11}^{\text{CL}}(0, \mathbf{x}) = \frac{4}{L_1 L_2 L_3} \sum_p \frac{1}{D(\mathbf{p})^2} \left[\cos(ap_1) \left(\hat{\mathbf{p}}^2 - 2\hat{p}_1^2 + E(\mathbf{p})^2 \right) - 2a\hat{p}_1^2 E(\mathbf{p}) \right] \tag{B9}$$

with

$$A(\mathbf{p}) = 1 + am + \frac{1}{2}a^2 \hat{\mathbf{p}}^2, \quad B(\mathbf{p}) = m^2 + (1 + am)\hat{\mathbf{p}}^2 + \frac{1}{2}a^2 \sum_{k<l} \hat{p}_k \hat{p}_l^2. \tag{B10}$$

$$C(\mathbf{p}) = \frac{1}{2}a\hat{\mathbf{p}}^2 + m - \frac{aB(\mathbf{p})}{2A(\mathbf{p})}, \quad D(\mathbf{p}) = \sqrt{B(\mathbf{p})(4A(\mathbf{p}) + a^2 B(\mathbf{p}))}, \tag{B11}$$

$$E(\mathbf{p}) = C(\mathbf{p}) + D(\mathbf{p}) / (2A(\mathbf{p})), \quad \omega_p = \frac{2}{a} \operatorname{asinh} \left(\frac{a}{2} \sqrt{B(\mathbf{p})/A(\mathbf{p})} \right). \tag{B12}$$

This representation is useful to calculate the $T = 0$ vector correlator (in which case the L_i can be sent to infinity) and the screening correlator at finite T (in which case the direction \mathbf{e}_0 is interpreted as a spatial direction, while one of the directions \mathbf{e}_k is interpreted as the Matsubara cycle). For the correlator of two local vector currents, see [38].

-
- [1] P. Arnold, W. Florkowski, Z. Fodor, P. Foka, J. Harris, et al., PoS **ConfinementX**, 030 (2012).
[2] M. H. Thoma, J.Phys. **A42**, 214004 (2009), 0809.1507.
[3] C. Gale (2012), 1208.2289.
[4] C. Shen, U. W. Heinz, J.-F. Paquet, and C. Gale (2013), 1308.2440.
[5] B. B. Brandt, A. Francis, H. B. Meyer, and H. Wittig, JHEP **1303**, 100 (2013), 1212.4200.
[6] H.-T. Ding, A. Francis, O. Kaczmarek, F. Karsch, E. Laermann, et al., Phys.Rev. **D83**, 034504 (2011), 1012.4963.
[7] A. Amato, G. Aarts, C. Allton, P. Giudice, S. Hands, et al. (2013), 1307.6763.
[8] J. Ghiglieri, J. Hong, A. Kurkela, E. Lu, G. D. Moore, et al., JHEP **1305**, 010 (2013), 1302.5970.
[9] E. M. Purcell, *Electricity and Magnetism* (Cambridge University Press, 1963).
[10] J. Hong and D. Teaney, Phys. Rev. **C82**, 044908 (2010), 1003.0699.
[11] R. Baier, P. Romatschke, D. T. Son, A. O. Starinets, and M. A. Stephanov, JHEP **04**, 100 (2008), 0712.2451.
[12] P. Romatschke and D. T. Son, Phys. Rev. **D80**, 065021 (2009), 0903.3946.
[13] O. Philipsen and C. Schaefer, **Lattice13** (2013).
[14] S. Weinberg, *The Quantum theory of fields. Vol. 1: Foundations* (Cambridge University Press, 1995).
[15] J. I. Kapusta and C. Gale, *Finite-temperature field theory: Principles and applications* (Cambridge University Press, 2006), 428.
[16] K. A. Olive, AIP Conf.Proc. **1548**, 116 (2012).
[17] K. G. Wilson, Phys. Rev. **D10**, 2445 (1974).
[18] K. Jansen and R. Sommer (ALPHA collaboration), Nucl.Phys. **B530**, 185 (1998), hep-lat/9803017.
[19] M. Hasenbusch, Phys.Lett. **B519**, 177 (2001), hep-lat/0107019.
[20] M. Hasenbusch and K. Jansen, Nucl.Phys. **B659**, 299 (2003), hep-lat/0211042.
[21] M. Marinkovic and S. Schaefer, PoS **LATTICE2010**, 031 (2010), 1011.0911.
[22] <http://luscher.web.cern.ch/luscher/DD-HMC/index.html> (2010).
[23] P. Fritzsche, F. Knechtli, B. Leder, M. Marinkovic, S. Schaefer, et al., Nucl.Phys. **B865**, 397 (2012), 1205.5380.

- [24] <https://twiki.cern.ch/twiki/bin/view/CLS/WebIntro> (2010).
- [25] B. B. Brandt, A. Francis, H. B. Meyer, O. Philipsen, and H. Wittig (2012), 1210.6972.
- [26] S. Capitani, M. Della Morte, G. von Hippel, B. Knippschild, and H. Wittig, PoS **LATTICE2011**, 145 (2011), 1110.6365.
- [27] M. Bochicchio, L. Maiani, G. Martinelli, G. C. Rossi, and M. Testa, Nucl. Phys. **B262**, 331 (1985).
- [28] M. Lüscher, S. Sint, R. Sommer, P. Weisz, and U. Wolff, Nucl.Phys. **B491**, 323 (1997), hep-lat/9609035.
- [29] M. Guagnelli et al. (ALPHA Collaboration), Nucl.Phys. **B595**, 44 (2001), hep-lat/0009021.
- [30] M. Della Morte, R. Hoffmann, and R. Sommer, JHEP **0503**, 029 (2005), hep-lat/0503003.
- [31] M. Della Morte, R. Sommer, and S. Takeda, Phys.Lett. **B672**, 407 (2009), 0807.1120.
- [32] M. Della Morte et al. (ALPHA Collaboration), Nucl.Phys. **B729**, 117 (2005), hep-lat/0507035.
- [33] M. Della Morte, R. Hoffmann, F. Knechtli, R. Sommer, and U. Wolff, JHEP **0507**, 007 (2005), hep-lat/0505026.
- [34] M. Lüscher, S. Sint, R. Sommer, and P. Weisz, Nucl. Phys. **B478**, 365 (1996), hep-lat/9605038.
- [35] S. Sint and P. Weisz, Nucl.Phys. **B502**, 251 (1997), hep-lat/9704001.
- [36] A. Francis, B. Jäger, H. B. Meyer, and H. Wittig, Phys.Rev. **D88**, 054502 (2013), 1306.2532.
- [37] M. Laine and M. Vepsäläinen, JHEP **02**, 004 (2004), hep-ph/0311268.
- [38] G. Aarts and J. M. Martinez Resco, Nucl. Phys. **B726**, 93 (2005), hep-lat/0507004.
- [39] The energy level extracted in this way does not necessarily correspond to a stable vector particle.